Ceramic bricks containing Ni ions from contaminated biomass used as an adsorbent

Daiana Simón
Instituto de Investigaciones en Ciencia y Tecnologia de Materiales
Nancy Quaranta
Universidad Tecnologica Nacional
Sebastián Gass
Instituto de Investigaciones en Ciencia y Tecnologia de Materiales
Raúl Procaccini
Instituto de Investigaciones en Ciencia y Tecnologia de Materiales
Adrián Cristóbal (acristobal@fi.mdp.edu.ar)
Instituto de Investigaciones en Ciencia y Tecnologia de Materiales

Research

Keywords: Toxic metals, Wood waste, Adsorption, Porous bricks, Cooked ceramic immobilization, Sustainability

Posted Date: October 14th, 2020

DOI: https://doi.org/10.21203/rs.3.rs-35284/v5

Version of Record: A version of this preprint was published on October 20th, 2020. See the published version at https://doi.org/10.1186/s42834-020-00067-3.

Abstract

This article shows how pine sawdust residues can be used to adsorb nickel ions from synthetic solutions and then to produce porous bricks for civil construction using a mixture of natural clay and biomass containing the adsorbed metals. The adsorption tests were performed by mixing NiCl2 solutions with pine sawdust during a fixed stirring period of 24 h. The set was filtered and the filtrate was analysed. Highest efficiency adsorbate/adsorbent ratio was 50 mL of 1 M NiCl2 solution and 20 g L-1 of pine sawdust. This was the contaminated biomass sample used in the manufacture of the bricks. This paper analyses the properties of the bricks achieved and compares them with bricks without added biomass, porous bricks containing zinc and commercial bricks. The obtained values of bulk density, apparent specific weight, apparent porosity, water absorption, apparent volume, weight loss on ignition, compressive strength, flexural modulus of rupture and efficiency retention of metal in the brick, demonstrate that the ceramic pieces obtained are optimal for construction.

Introduction

Heavy metals are the main inorganic micro pollutants, and their discharge into aquatic bodies affects the ecosystem and health, due to their toxicity and possible carcinogenic effect. The lack of biodegradability of these pollutants produces their bioaccumulation and persistence in the environment, and their danger is given both by the concentrations in which they may be present, as well as by their chemical behaviour. The anthropogenic sources of heavy metals are very varied, with the metal finishing industry being the most contributor due to the large number of companies that integrate and its geographical dispersion [1-3].

Nickel is a dangerous heavy metal. The World Health Organization states that 0.07 mg L^{-1} is the allowed limit of this contaminant in water for consumption [4]. This contaminant can cause adverse effects on the blood, kidneys, bronchi, lung and stomach. The main sources of nickel are the stainless steel and alloy, electroplating, catalysts and Ni/Cd industries. The reduction of nickel concentration in water and wastewater is of great interest due to the current increase in demand of such emitting industries [5, 6].

The most commonly used conventional methods for removing Ni(II) and other toxic metals from wastewater are chemical precipitation, solvent extraction, ion exchange, flotation, adsorption with activated carbon, among others [6, 7]. However, to date, there is no low-cost technology that allows to reach very low levels of these pollutants. In this situation, the removal of heavy metal ions using low-cost adsorbents has recently gained relevance [8-10]. Research has shown that materials of biological origin, such as biomass of algae, fungi and bacteria, as well as residues and by-products from the agro-industrial sector, can retain heavy metal ions [3, 11]. Bioadsorption of pollutants from cellulosic biomass residues has attracted attention because it not only allows the removal of heavy metals in industrial effluents, but also treats agricultural waste that is produced today in huge tons and does not have a specific use [12]. In this sense they have been studied as adsorbents, rice husk [13, 14], sawdust [15, 16], fruit peels [17, 18] and others [19, 20].

Heavy metals are attracted to the adsorbent through a complex process involving mechanisms such as surface adsorption (by Van Der Waals forces, dipole interactions, or hydrogen bonding), interstitial adsorption (through the pores of the material), ion exchange adsorption (between metal ions and adsorbent ions, facilitated by carboxyl groups and hydroxyl), by electrostatic forces (related to the pH of the solution and the zero charge point of the adsorbent), complexation (through carboxylate groups, amides, phosphate, thiols and hydroxide), precipitation, among others [10, 21]. The availability of the active biomass sites is influenced by the kind of biomass, the metallic solution, the pH, the temperature, the contact time and the stirring speed of the mixture. [10, 22].

Currently, there are researches on the production of porous ceramic bricks from the incorporation of agroindustrial biomass residues. These residues act as pore-forming agents because at the sintering temperatures their combustion produces gases and ashes. For this purpose, residue of olive [23], sunflower and wheat [24], fruit pits [25], vine [26] and rice [27] have been investigated.

The aim of this article is to adsorb Ni(II) ions on wood industry residues (pine sawdust) and then use these new contaminated residues as an aggregate in clay to generate optimal porous ceramic matrices for civil construction, which will contain retained metals. The metals will be immobilized in the ceramic pieces, stabilizing them and reducing their release, solubility and toxicity. In this way, the negative effects on the environment are minimized [28, 29].

Materials And Methods

2.1. Adsorbate

The metal solutions used in this study (0.125 to 1 mol L^{-1}) were prepared by dissolving appropriately measured amounts of $NiCl_2$ x 6 H_2O salt (analytical grade, Cicarelli) in distilled water.

2.2. Bioadsorbent

The adsorbent used was the residue obtained from the processing of Pinus elliottii wood in a sawmill from the north east area of Argentina. This residue was sieved to obtain particles smaller than 1 mm. It was then boiled with distilled water for 90 min, filtered and washed repeatedly. Finally, the material was dried in an oven at 50 °C.

2.3. Batch adsorption experiments

A qualitative study of the adsorption at different times of Ni(II) ions of solutions 0.25 mol L^{-1} of $NiCl_2$ in contact with 10 g L^{-1} of pine sawdust was carried out. 50 mL metallic solutions prepared at pH 5-6 (PH/MV/°C HANNA HI 8424), were put in contact with pine sawdust by constant stirring at room temperature of 200 rpm (SK-0330-Pro shaker). Then, each mixture was filtered and the solid residues were dried at 50 °C. The pH was chosen according to what is reported in the bibliography [10, 30], at higher pH values Ni(II) forms a complex with hydroxide ions, precipitating and decreasing adsorption, and

at a pH less than this value, H^+ can compete with ions of heavy metals by the active sites of the adsorbent and also, functional groups of the adsorbent that intervene in the adsorption process can be protonated (general positive charge on the adsorbent), generating an electrostatic repulsion on the positively charged metal ions leading to adsorption. This test was performed with the aim of estimating an optimal time for contact between heavy metal ions and pine sawdust biomass by means of X-ray fluorescence (XRF) measurements on the solids obtained from the filtrate. The tests were done in triplicate.

Subsequently, adsorption tests were performed at different concentrations of $NiCl_2$ from 0.125 to 1 mol L^{-1} and varying from 10 to 40 g L^{-1} the biomass residue content to determine in this way the most efficient adsorbate/adsorbent ratio used in the manufacture of ceramic pieces. For this, the amount of residual metal that was not adsorbed on the biomass and remained in the solution after the filtration process was quantified by UV-Vis Spectrophotometry (UV-Vis) at λ = 722 nm (this λ was chosen to reduce the signal obtained by the organic matter, in addition to making blank samples). The tests were done in triplicate. The adsorption efficiency (R) (%) of Ni(II) was calculated following Eq. (1) and the adsorption capacity (qe) (mg g^{-1}) was defined by Eq. (2):

See formulas 1 and 2 in the supplementary files.

where C_i and C (mg L^{-1}) are the initial and residual concentration of Ni(II); V (L) is the volume of solution and M (g) is the mass of the adsorbent. The amount C was determined by UV-Vis.

2.4. Bricks production and characterization

The bricks used to carry out the mechanical tests were made by mixing 100 g of clay from a natural quarry in eastern Buenos Aires and the biomass containing the adsorbed Ni(II) in a proportion of 20% by volume of clay. The particle size of the contaminated pine sawdust was less than 1 mm and the particle size of the clay was less than that of the biomass.

The adsorption sample used for the manufacture of bricks was the one representing the highest efficiency adsorbate/adsorbent ratio determined by the adsorption experiments.

For formation, a uniaxial pressure of 25 MPa was used, with the addition of 8 mL of water, in molds of 70 mm x 40 mm x 18 mm. After a drying period of 24 h in the environment, the green bricks were calcined at 950 °C for 3 h. The heating rate was 1 °C min^{-1} and the cooling rate was 5 °C min^{-1}.

The sintered ceramic pieces were physically characterized and their mechanical properties were evaluated in triplicate.

Weight loss on ignition (LOI) was determined. Also, apparent porosity (apP), together with bulk density (apD), apparent specific weight (apsW), water absorption (H_2OAbs) and apparent volume (apV), were determined following the Archimedes principle and based on the IRAM standard 1554.

Flexural modulus of rupture (MOR) and compressive strength (σstr) were evaluated in test specimens in accordance with the provisions of the IRAM 12587 standard and the IRAM 12586:2004 standard, respectively. The MOR was determined on rectified samples of 70 mm x 40 mm x 18 mm, submitted to a three-point bending test. The σstr was determined on rectified samples of 35 mm x 40 mm x 18 mm.

Leaching tests on 10 g of the bricks were carried out following the procedure described in EPA 1311 Toxicity Characteristic Leaching Procedure (TCLP) and in triplicate. The brick fragments were contacted with 20 times the volume of extraction solvent (leaching solution of pH 4.93 ± 0.05, prepared from 5.7 mL of acetic acid in 500 mL of distilled water, adding 64.3 mL of 1 N sodium hydroxide and diluting up to 1 L). The mixture was stirred at 50 rpm for 18 h. The system was filtered and the concentration of Ni(II) was determined on the filtered liquid by Atomic Absorption Spectrophotometry (AA).

2.5. Equipment

Thermogravimetric-differential thermal analysis (TGA-DTA): Shimadzu TGA-50 and Shimadzu DTA-50 equipment, with TA-50 WSI analyser. Thermal characterization of pine sawdust residues. Conditions: air flow, heating up to 1000 °C at a rate of 10 °C min^{-1} and approximately 20 mg of residue.

Scanning electron microscopy (SEM) - energy dispersive analysis of X-ray (EDS): SEM Philips 515 equipment, with energy dispersive analyser (EDAX-Phoenix). Microstructural characterization of pine sawdust residues. Determination of Ni(II) in the biomass after the adsorption process and in the manufactured bricks.

Fourier-transform infrared spectroscopy (FTIR) in attenuated total reflectance – ATR mode: Nicolet 6700, Thermo Electron Corp. equipment. Characterization of the functional groups present in the biomass of pine sawdust before and after the Ni(II) adsorption process.

X-ray diffraction (XRD): PANalytical X'Pert PRO equipment, with CuKα radiation (λ = 1.5406 nm). Characterization of pine sawdust before and after Ni (II) adsorption, and characterization of clay and bricks manufactured after the sintering process. Conditions: 40 kV and 40 mA

XRF: Panalytic Minipal2 PW4024 X-ray spectrometer with copper anode. Qualitative study on sawdust residues from the adsorption of Ni(II) ions as a function of time and qualitative study on the adsorbent from the adsorption of Ni(II) as a function of the initial concentration of metal. Characterization of manufactured bricks. Conditions: helium flux, voltage 20 KV, current 5 mA and time 100 sec.

UV-Vis: Shimadzu 3600 Plus UV-VIS-NIR spectrophotometer at λ = 722 nm. Determination of the concentration of Ni(II) on the filtrates obtained in the adsorption tests.

Mechanical tests: Instron 8501 universal servo hydraulic testing machine. MOR determination. Conditions: room temperature, distance between supports 60 mm, speed of application of the load 0.5 mm min^{-1} in displacement control. σstr determination. Conditions: room temperature, load application speed of 8.25 KN min^{-1} in control per load.

AA: Shidmadzu AA 6800 - Flame mode. Determination of the concentration of Ni(II) on the filtrates obtained in the leaching tests.

Results And Discussion

3.1. Bioadsorbent characterization

Thermal analysis by TGA-DTA for pine sawdust is presented in Fig. 1 It is very important to know the behaviour of biomass as the temperature rises, since this is closely related to the properties that the brick will reach when sintered.

The DTA diagram shows an endothermic peak at 52 °C and a small exothermic peak at 263 °C assigned to the loss of water from the sample and the combustion of volatile components, respectively. In addition, in this diagram it is also possible to recognize two exothermic peaks at 327 °C and 488 °C, attributed to the decomposition of hemicellulose (roasted in wood called active pyrolysis), and decomposition of cellulose (passive pyrolysis) and lignin (active and passive pyrolysis), respectively.

It is possible to observe three major mass losses in the TGA diagram, a first loss up 230 °C corresponding to the loss of moisture and the decomposition of volatile components, a second loss up to 311 °C assigned to hemicellulose (to give lower weight compounds molecular, mainly acetic acid), and, finally, a loss of mass up to 502 °C assigned to cellulose and lignin (to finally give CO_2, H_2O and ash). Hemicellulose combustion occurs at lower temperatures due to its linear structure with short side chains. Cellulose and lignin have more complex and stronger structures, with associated dispositions and aromatic compounds, so they have greater resistance to heat.

These results demonstrate that, during the sintering of the ceramic pieces, the biomass added to the clay mix the whole will gradually calcine as the temperature of the oven increases. This will allow the gases formed to diffuse slowly and the fired bricks will not crack. From the data obtained from the TGA analysis, it is possible to obtain an estimated composition for pine sawdust residues. This composition is detailed in Table 1. In particular, the value of inorganic ash was also carried out by the ASTM E 1755-01 standard method and the value obtained, 2.9%, is similar to that obtained by thermogravimetric analysis.

Figure 2 shows two SEM images of pine sawdust waste used in adsorption experiments. The images show that pine sawdust has a fibrous and irregular structure with pores smaller than 50 microns and elongated particles. These surface characteristics could make the adsorption of heavy metals possible.

Figure 3 shows the FTIR spectrum of the biomass. FTIR was used for the qualitative analysis of the biomass residues of pine sawdust and to identify the functional groups that could participate in the adsorption of contaminating metals. It is possible to observe the presence of bands corresponding to stretches O-H (3344 cm^{-1}) of hydroxyl groups of phenol, C-H of aromatic methoxide group (2922 cm^{-1}), and vibration of aromatic ring (1508 cm^{-1}), assigned to lignin; stretching C=O (1600 cm^{-1}), and C-OH and C-H (1103 cm^{-1}), assigned to cellulose and lignin; C-H flexion of the methyl group (1327 cm^{-1}), and

stretching C-O, C=C and C-C-O (1032 cm^{-1}), assigned to hemicellulose, cellulose and lignin; and asymmetric stretching C-O-C (1158 cm^{-1}) and glyosidic bond (830 cm^{-1}), corresponding cellulose and hemicellulose. Similar results have been reported in bibliography [31]. The observed peak around 2359 cm^{-1} of wave number corresponds to the residual signal of the asymmetric stretch O=C=O of the CO_2 that the target failed to completely eliminate.

Figure 4 shows the XRD diagram of the pine sawdust residue, with the characteristic peaks at 16.2 °, 22.4 ° and 34.8 ° typical of semi-crystalline cellulose. In addition, a peak at 26.5 ° corresponding to SiO_2 (quartz) and three other peaks of $CaCO_3$ (calcite) at 24.5 °, 28.2 ° and 38.2 ° are observed in the diagram.

3.2. Qualitative study by XRF of the adsorption of Ni(II) ions as a function of time

Figure 5 shows how the amount of Ni(II) adsorbed increases as the stirring time between the Ni(II) solution and the pine sawdust biomass increases. This process was performed to estimate the optimal contact time for a certain concentration of heavy metal and a certain amount of sawdust. The analysis was performed by XRF on the solids obtained after remaining in contact with the $NiCl_2$ solution during each of the stirring times studied. Figure 5 shows that Ni(II) adsorption on pine sawdust increases with contact time because, initially, there is a greater availability of active biomass sites. After a certain time, a plateau is reached which represents a stability in the adsorption of nickel ions. This shows a successive occupation of the active sites of pine sawdust by the pollutant, which causes, after a time, the adsorption to decrease. According to the results obtained, the stirring time for the adsorption tests was 24 h to ensure arrival at the plateau.

3.3. Effect of the initial concentration metal and dose of bioadsorbent

Ni(II) adsorption tests were carried out by modifying the initial concentration of the metallic solutions, but maintaining the volume of the solution, and studying adsorption on 3 different amounts of biomass, 10, 20 and 40 g L^{-1}. After a 24 h stirring time, the mixtures were filtered and the remaining solutions were analysed to determine their residual nickel concentration. Figure 6a shows the relationship between adsorbent dose, initial adsorbate concentration, and Ni(II) adsorption efficiency. R values are higher for low $NiCl_2$ concentrations because there are many binding sites available in pine sawdust biomass but then decrease for all residue doses studied. In Fig. 6b it is possible to observe how at higher initial concentrations of $NiCl_2$ greater adsorption capacity. As the concentration of metal ions increased, the collisions between these and the adsorbent increased. Finally, it seems that at high metal concentrations there is a tendency to reach a plateau. According to Fig. 6b, in the concentration range studied, at the concentration of 1 mol L^{-1} $NiCl_2$ (5.87 x 10^4 mg L^{-1} Ni^{+2}) the adsorption capacity is greater. This value increases when the adsorbent dose of 20 g L^{-1} is used. Furthermore, it is observed in Fig. 6a that when the amount of biomass doubles from 10 g L^{-1} to 20 g L^{-1}, the R increases 2.5 times, but when the sawdust dose is doubled again, the R increases only 1.5 times. Therefore, the adsorbate/adsorbent ratio of 1 mol

L^{-1} $NiCl_2$ and 20 g L^{-1} sawdust was considered the most efficient and was then used in the construction of clay bricks.

Figure 7 shows qualitative XRF analysis of the amount of Ni(II) absorbed in the solids obtained after contact with $NiCl_2$ solutions for a concentration range of 0.125 to 1 mol L^{-1} of $NiCl_2$ using a dose of 20 g L^{-1} of adsorbent. As the initial concentration of $NiCl_2$ increases, the nickel adsorbed on the pine sawdust increases and there is a tendency to reach a plateau that marks the saturation of the biomass. This $NiCl_2$ concentration is 1 mol L^{-1}.

In Fig. 8, the FTIR spectrum of pine sawdust is compared with that measured after 24 h of stirring with a solution of 1 mol L^{-1} of $NiCl_2$. A slight change in the position and intensity of the bands in the biomass residue can be observed after the metal adsorption, due to the probable complexation or electrostatic interaction reactions and the Van der Waals forces. It is important to highlight the evidence of new bands at 3487, 1606, 717 cm^{-1} (indicated with * in Fig. 8), visible from the 1 mol L^{-1} concentration of $NiCl_2$ and belonging to this compound, giving an indication of its adsorption as such in the biomass.

The Fig. 9 shows the XRD of sawdust after the sorption process with 1 mol L^{-1} $NiCl_2$. It is from this concentration of $NiCl_2$ that it can be seen, in addition to the peaks corresponding to sawdust, peaks belonging to $NiCl_2(H_2O)_2$ in concordance with what was observed in Fig. 8.

The biomass electron micrographs after adsorption are shown in Fig. 10. Agglomerates of pine sawdust particles exceed 25 microns. From EDS, the homogeneous presence of adsorbed Ni can be identified. Semi-quantitative chemical analysis by EDS for the pine sawdust residues after the adsorption process shows that the percentage composition by mass, without considering the carbon content in the sample, is 22.88% oxygen, 0.18% silicon, 36.72% chlorine and 40.22% nickel.

3.4. Characterization and evaluation of the bricks

The composition of the clay used as raw material in the manufacture of the bricks is the same as that used by a local brick maker and is shown in Fig. 11.

Figure 12 shows the physical appearance of the manufactured sintered ceramic pieces, (a) without added residue (ARC), and (b) with added 20% by volume of sawdust containing nickel adsorbed (AN20). Each AN20 brick weighs approximately 90 g and an estimate of its nickel content from Fig. 6 is 0.8 g. Both pieces are compact, but ARC has a reddish color due to the Fe present in the clay, while AN20 has a darker color that could be contributed by high levels Ni(II) retained on the biomass and then immobilized in the cooked brick.

Figure 13 shows the DRX obtained for AN20 after cooking. It is possible to observe the presence of SiO_2 together with peaks corresponding to numerous secondary phases because the clay used was obtained from natural quarries. Furthermore, it is possible to observe peaks corresponding to NiO.

Figure 14 shows the XRF diagrams of the AN20 and ARC bricks together with a commercial brick (COM). The presence of lines corresponding to nickel corroborates that the metal remains in the clay matrix after the sintering process.

The EDS images of powder AN20 are shown in Fig. 15. These images allow to corroborate the presence and immobilization of Ni after the sintering process. Semi-quantitative chemical analysis by EDS for AN20 shows that the percentage composition by mass, without considering the carbon content in the sample, is 42.04% oxygen, 0.79% sodium, 1.07% magnesium, 11.48% aluminum, 27.88% silicon, 2.25% potassium, 1.77% calcium, 0.61% titanium, 8.32% iron and 3.79% nickel.

Table 2 shows the average values obtained from LOI and the parameters determined from the apparent porosity test of the manufactured bricks. The LOI was greater for AN20 than for ARC due to the combustion, during sintering, of the aggregate biomass. This combustion of sawdust waste generates a greater apP observed in ceramic pieces made from clay and the addition of 20% biomass. Higher values of apP and H_2OAbs determine lower values of apD and apsW for AN20. In addition, the mechanical properties of the AN20 and ARC ceramic matrices were evaluated and the average values obtained are presented in Table 2. The average values of σstr obtained are within the commercially required standards according to IRAM 12566-1:2005, "the bricks must have a characteristic compressive strength equal to or greater than 4 MPa". In addition, in Argentina, CIRSOC 501R - 2007 regulates the use in construction, and sets a lower limit of 5 MPa. These σstr values were lower for AN20 than for ARC due to aggregate biomass. This same behavior is observed in MOR. According to the literature [32], the MOR varies between 10 and 30% of the σstr, so AN20 still has a MOR value within the appropriate parameters of the market (MOR = 23 % σrot).

Very similar values of these properties were obtained for the brick manufactured from sawdust with Zn(II) adsorbed (AZ20) [33]. Also, in Table 2, the values for a COM are presented. AN20 has superior physical and mechanical characteristics compared to COM.

A common concern when adding contaminated waste to fired brick is the possible migration of these contaminants into the environment. In this sense, it is important to evaluate the leachability of the manufactured AN20 ceramic matrices. National Law 24051 and its regulatory decree establish that leachates in dangerous products must be analyzed in accordance with TCLP. The measurements were obtained in triplicate following the protocol (using fragments of AN20 and a solution of pH 4.93 ± 0.05 as extraction solvent, determined from the sample's alkalinity according to TCLP). Table 3 shows the average Ni(II) result obtained in the leached liquid. This value was less than 0.05 mg L^{-1} nickel and was compared with the maximum concentrations allowed according to Decree No. 2020 of 2007 of Law No. 2214 of the City of Buenos Aires (CABA), US EPA Code of Federal Regulations 2012 and the regulations in force in Spain and China. Therefore, the metal concentrations obtained by TCLP of AN20 are below the established maximum. A previous investigation has allowed obtaining similar behavior in AZ20 bricks [33]. These tests demonstrate that during the brick firing process, biomass residues are destroyed and heavy metals could encapsulate in the clay matrix, form oxides, and interact with silicon, iron, or

aluminum oxides in the clay to form minerals stable, according to the literature [34, 35]. The phase transformations and the evolution of the heavy metals during the firing of the ceramic pieces determine the fixation of the contaminants. However, the mechanism of immobilization of heavy metals during the sintering process has not yet been understood [36].

The calculation of the efficiency of the retention is made according to the Eq. 3 [37]

See formula 3 in the supplementary files.

where, ER = efficiency retention of metal in the brick (%), MMIB = mass of metal incorporated in AN20 and MML = mass of metal extracted in the leachate. M_{MIB} is estimated from the nickel mass adsorbed by pine sawdust in the ratio of highest efficiency selected and corrected for the mass of sawdust added as pore-forming agent in AN20. M_{ML} is estimated from the nickel concentration in the leachate corrected for the mass of the entire brick. ER for AN20 bricks is 99.99%.

Therefore, it is possible to immobilize Ni(II) in fired clay bricks and thus reuse the pine sawdust previously used as an adsorbent of these contaminants. In addition, a common paint such as latex, could act as an additional "barrier" that guarantees the non-leaching of Ni from inside the brick [28]

Conclusions

Pine sawdust generated by the timber industry was evaluated as an adsorbent of synthetic Ni(II) solutions. This residue, without a specific use at present, showed the ability to retain the ions of the heavy metal studied. In this way, pine sawdust constitutes a simple and low-cost system for wastewater treatment. The adsorption tests show that the most efficient adsorbate/adsorbent combination was found to be 20 g L^{-1} of sawdust and an initial $NiCl_2$ concentration of 1 mol L^{-1}.

The novelty is to use this new contaminated biomass in the manufacture of porous clay bricks, immobilizing heavy metals and minimizing the impact on the environment.

The sintered bricks presented values of apP and mechanical characteristics within the market requirements. In addition, TCLP tests show a ER close to 100%, which determines an excellent immobilization of Ni(II) within the ceramic pieces.

With these results, it would be possible to respond to the needs of the industry that generates contaminated effluents and of the agribusiness that generates biomass waste without a specific use and considerably reducing the negative implications on the environment.

Declarations

Availability of data and materials

All data generated or analyzed during this study are included in this published article or request the corresponding author.

Competing interests

The authors declare they have no competing interests.

Funding

This work was supported by Consejo Nacional de Investigaciones Científicas y Técnicas (CONICET), Universidad Nacional de Mar del Plata (UNMdP), Comisión de Investigaciones Científicas de la Provincia de Buenos Aires (CICPBA), Universidad Tecnológica Nacional (UTN) and Agencia Nacional de Promoción Científica y Tecnológica (ANCyT).

Authors' contributions

DS carried out the experimental work, processed the data obtained and wrote the document. NQ participated in the discussion of the results. SG collaborated with the experimental work and participated in the discussion of the results. RP collaborated with the experimental work and participated in the discussion of the results. AC coordinated the investigative work and wrote the document.

Acknowledgements

Not applicable.

Authors' information (optional)

Not applicable.

References

1. Tchounwou PB, Yedjou CG, Patlolla AK, Sutton DJ. Heavy Metal Toxicity and the Environment. Experientia Supplementum. 2012;101:133-64.
2. Saha N, Rahman MS, Ahmed MB, Zhou JL, Ngo HH, Guo W. Industrial metal pollution in water and probabilistic assessment of human health risk. J of Environmental Manag. 2017;185:70–
3. Vardhan KH, Kumar PS, Panda RC. A review on heavy metal pollution, toxicity and remedial measures: Current trends and future perspectives. J of Mol Liq. 2019;290:111197.
4. Chowdhury S, Mazumder MAJ, Al-Attas O, Husain T. Heavy metals in drinking water: Occurrences, implications, and future needs in developing countries. Sci of the Total Environ. 2016;569–70:476–
5. Tejada-Tovar C, Villabona-Ortiz A, Garcés-Jaraba L. Adsorción de metales pesados en aguas residuales usando materiales de origen biológico. Tecno Lógicas. 2015;18:109–23 [in Spanish].
6. Carolin CF, Kumar PS, Saravanam A, Joshiba GJ, Naushad M. Efficient techniques for the removal of toxic heavy metals from aquatic environment: A review. J of Environmental Chem Eng. 2017;5:2782–

7. Cuin ZX, Ren QK, Al SS, Bian DJ. Research progress in heavy metal wastewater treatment and recovery. Environmental Sci & Technol. 2010;33:375–
8. Yang JG. Heavy metal removal and crude bio-oil upgrading from Sedum plumbizincicola harvest using hydrothermal upgrading process. Bioresour Technol. 2010;101:7653–
9. Malik DS, Jain CK, Yadav AK. Removal of heavy metals from emerging cellulosic low-cost adsorbents: a review. Appl W Sci. 2017;7:2113–
10. Joseph L, Jun B, Flora JRV, Park CM, Yoon Y. Removal of heavy metals from water sources in the developing world using low-cost materials: A review. Chemosphere. 2019;229:142–
11. Afroze S, Sen TK. A Review on Heavy Metal Ions and Dye Adsorption from Water by Agricultural Solid Waste Adsorbents. W Air and Soil Pollut. 2018;229:1–
12. Zuin VG, Ramin LZ. Green and Sustainable Separation of Natural Products from Agro-Industrial Waste: Challenges, Potentialities, and Perspectives on Emerging. Topics in Curr Chem. 2018;376:3–
13. Sobhanardakani S, Parvizimosaed H, Olyaie E. Heavy metals removal from wastewaters using organic solid waste-rice husk. Environmental Sci and Pollut Res.2013;20:5265–
14. Lata S, Samadder SR. Removal of Heavy Metals Using Rice Husk: A Review. International J of Environmental Res and Development. 2014;4:165–
15. Demcaka S, Balintovaa M, Hurakovab M, Frontasyevac MV, Zinicovscaiac I, Yushin N. Utilization of poplar wood sawdust for heavy metals removal from model solutions. Nova Biotechnologica et Chimica. 2017;16:26–
16. Mahmood-ul-Hassan M, Yasin M, Yousra M, Ahmad R, Sarwar, S. Kinetics, isotherms, and thermodynamic studies of lead, chromium, and cadmium bio-adsorption from aqueous solution onto Picea smithiana sawdust. Environmental Sci and Pollut Res. 2018;25:12570–
17. Romero-Cano LA, García-Rosero H, González-Gutiérrez LV, Baldenegro-Pérez LA, Carrasco-Marín F. Functionalized adsorbents prepared from fruit peels: Equilibrium, kinetic and thermodynamic studies for copper adsorption in aqueous solution. J of Clean Prod. 2017;162:195–
18. Vilardi G, Di Palma L, Verdone Sapienza N. Heavy metals adsorption by banana peels micro-powder: Equilibrium modeling by non-linear models. Chin J of Chem Eng. 2018;26:455–
19. Anastopoulos I, Karamesouti M, Mitropoulos AC, Kyzas GZ. A review for coffee adsorbents. J of Molecular Liquids. 2017;229:555–
20. Wierzba S, Kłos A. Heavy metal sorption in biosorbents - Using spent grain from the brewing industry. J of Clean Prod. 2019;225:112–
21. Dai Y, Sun Q, Wang W, Lu L, Liu M, Li J, et al. Utilizations of agricultural waste as adsorbent for the removal of contaminants: A review. Chemosphere. 2018;211:235–
22. Ahmed JK, Ahmaruzzaman M. A review on potential usage of industrial waste materials for binding heavy metal ions from aqueous solutions. J of W Process Eng. 2016;10:39–
23. De la Casa JA, Romero I, Jiménez J, Castro E. Fired clay masonry unit's production incorporating two-phase olive mill waste (alperujo). Ceram International. 2012;38:5027–

24. Bories C, Aouba L, Vedrenne E, Vilarem G. Fired clay bricks using agricultural biomass wastes: Study and characterization. Construction and Build Mater. 2015;91:158–
25. Barbieri L, Andreola F, Lancellotti L, Taurino R. Management of agricultural biomass wastes: Preliminary study on characterization and valorization in clay matrix bricks. Waste Manag. 2013;33:2307–
26. Velasco PM., Ortiz MPM., Giró MAM., Melia DM., Rehbein JH. Development of sustainable fired clay bricks by adding kindling from vine shoot: Study of thermal and mechanical properties. Appl Clay Sci. 2015;107:156–
27. Mohanta K, Kumar A, Parkash O, Kumar D. Processing and properties of low-cost microporous alumina ceramics with tailored porosity and pore size fabricated using rice husk and sucrose. J of the Eur Ceram 2014;34:2401–12.
28. Bertini L, Dwek M, Pastore I, Correnti A. Inmovilización en Cemento de óxidos de metales pesados: revalorización de un residuo con fines sociales y ambientales. In: Ingeniería 2014, Latinoamerica y el caribe. Buenos Aires; 2014 Nov 4-6.
29. Zhang M, Chen CM, Linqiang W, Wu Q. Use of electroplating sludge in production of fired clay bricks: Characterization and environmental risk evaluation. Construction and Build Mater. 2018;159:27–
30. Rafatullah M, Sulaiman O, Hashim R. A. Ahmad, Adsorption of copper (II), chromium (III), nickel (II) and lead (II) ions from aqueous solutions by meranti sawdust. J of Hazard Mater. 2009;170:969–
31. Xu F, Yu J, Tesso T, Dowel F, Wang D. Qualitative and quantitative analysis of lignocellulosic biomass using infrared techniques: a mini-review. Appl Energy. 2013;104:801–
32. Afanador García N, Guerrero Gómez G, Monrroy Sepúlveda R. Propiedades físicas y mecánicas de ladrillos macizos cerámicos para mampostería. Ciencia e ingeniería Neogranadina. 2012;22:43–58 [in Spanish].
33. Simón D, Quaranta N, Medici S, Costas A, Cristóbal A. Immobilization of Zn (II) ions from contaminated biomass using ceramic matrices. J of Hazard Mater. 2019;373:687–
34. Zhang M, Chen Ch, Mao L, Wu Q. Use of electroplating sludge in production of fired clay bricks: Characterization and environmental risk evaluation. Construction and Build Mater. 2018;159:27–
35. Ukwatta A, Mohajerani A. Leachate analysis of green and fired-clay bricks incorporated with biosolids. Waste Manag. 2017;66:134–
36. Li M, Su P, Guo Y, Zhang W, Mao L. Effects of SiO_2, Al_2O_3 and Fe_2O_3 on leachability of Zn, Cu and Cr in ceramics incorporated with electroplating sludge. J of Environmental Chem Eng. 2017;5:3143–
37. Yilmaz O, Kahraman U, Cokca E. Solidification/Stabilization of Hazardous Wastes Containing Metals and Organic Contaminants. J of Environmental Eng. 2003;130:366–

Tables

Table 1 Estimated percentage composition of pine sawdust waste from the TGA analysis.

Composition	%
Moisture and volatile	7.4
Hemicellulose	47.4
Cellulose and lignin	41.3
Inorganic ash	3.8

Table 2 Properties of sintered ceramic pieces and a commercial brick.

Brick	apD (g cm-^{3})	apsW (g cm-^{3})	apP (%)	H_2OAbs (%)	apV (cm^3)	LOI (%)	σstr (MPa)	MOR (MPa)
ARC	1.994 ± 0.001	1.997 ± 0.001	26.2 ± 0.2	13.1 ± 0.1	10.12 ± 0.06	8.6 ± 0.1	24.3 ± 0.1	2.8 ± 0.3
COM	1.37 ± 0.01	1.38 ± 0.01	44.2 ± 0.4	32.15 ± 0.05	13 ± 1	-	2.9 ± 0.1	1.7 ± 0.1
AN20	1.854 ± 0.003	1.857 ± 0.003	31.28 ± 0.02	16.85 ± 0.04	11.242 ± 0.006	13.9 ± 0.9	10.5 ± 0.1	2.41 ± 0.01
AZ20	1.84 ± 0.02	1.85 ± 0.02	31.4 ± 0.7	17.0 ± 0.5	10.58 ± 0.02	12.4 ± 0.7	9.7 ± 0.1	1.82 ± 0.07

Table 3. Results of the TCLP standard procedure of AN20 bricks. Comparison with limit concentrations of Ni(II).

Heavy metal	TCLP of AN20 (mg L^{-1})	Decree No. 2020 of 2007 of Law No. 2214 of the City of Buenos Aires (CABA) (mg L^{-1})	US EPA Code of Federal Regulations 2012 (mg L^{-1})	UNE-EN 12457-4 (Spanish standard) (mg L^{-1})	GB 5085.3-2007 (Chinese standard) (mg L^{-1})
Ni	< 0.05	5.0	Not Given	2.0 - 0.4	5.0

Figures

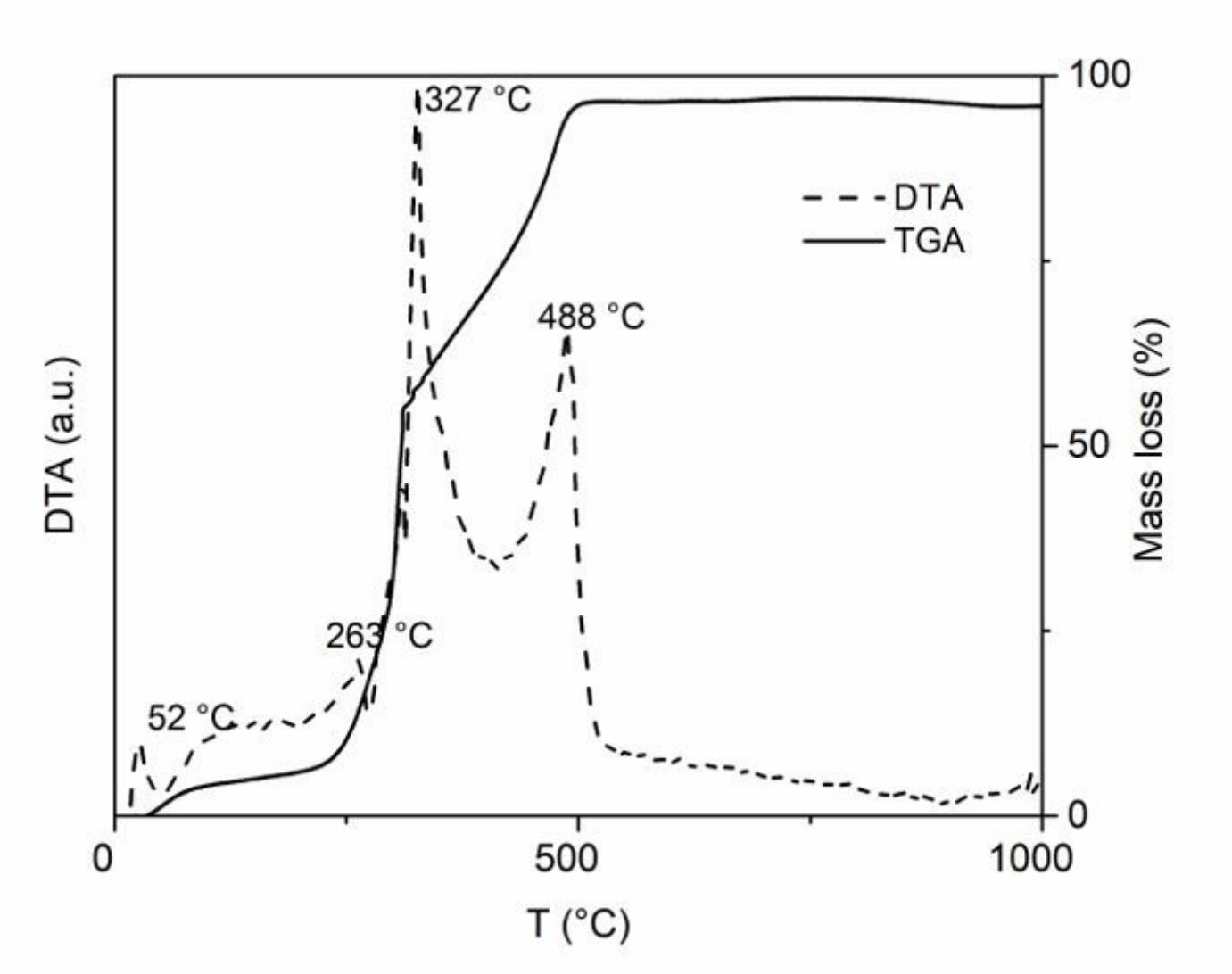

Figure 1

TGA-DTA of biomass residues from pine sawdust.

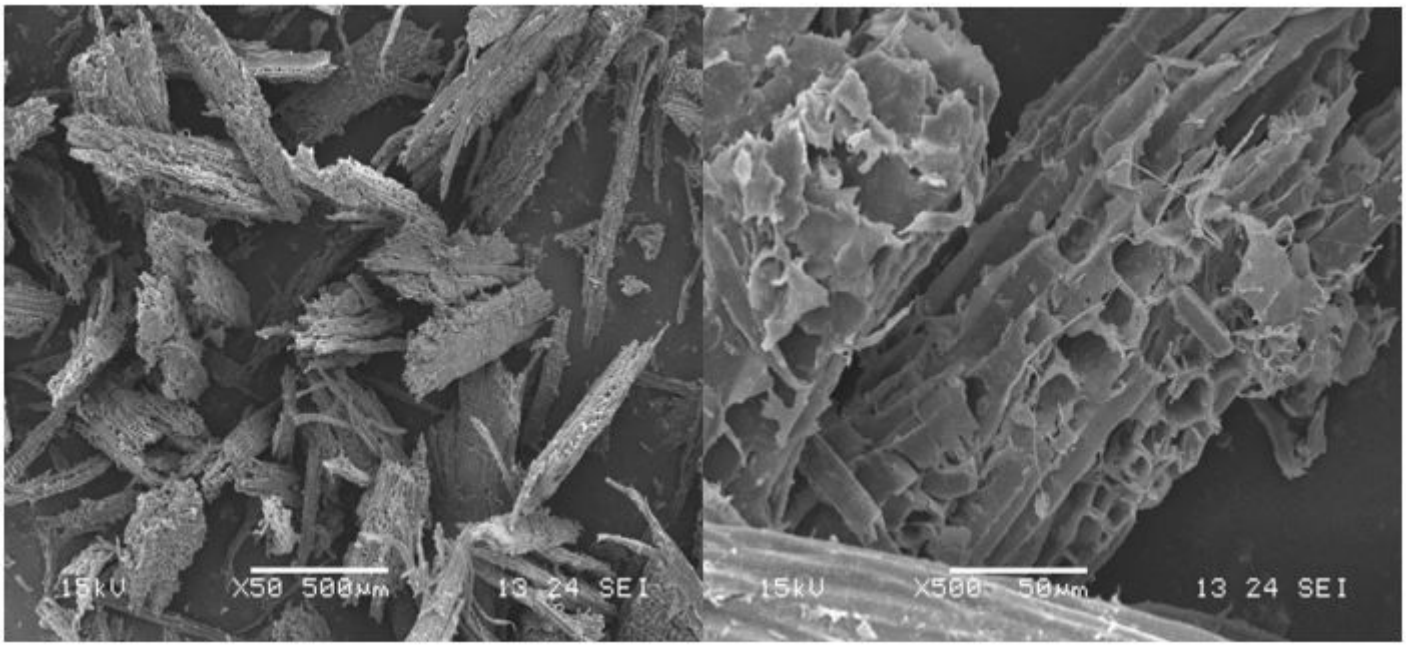

Figure 2

SEM images x 50 and x 500 of pine sawdust waste.

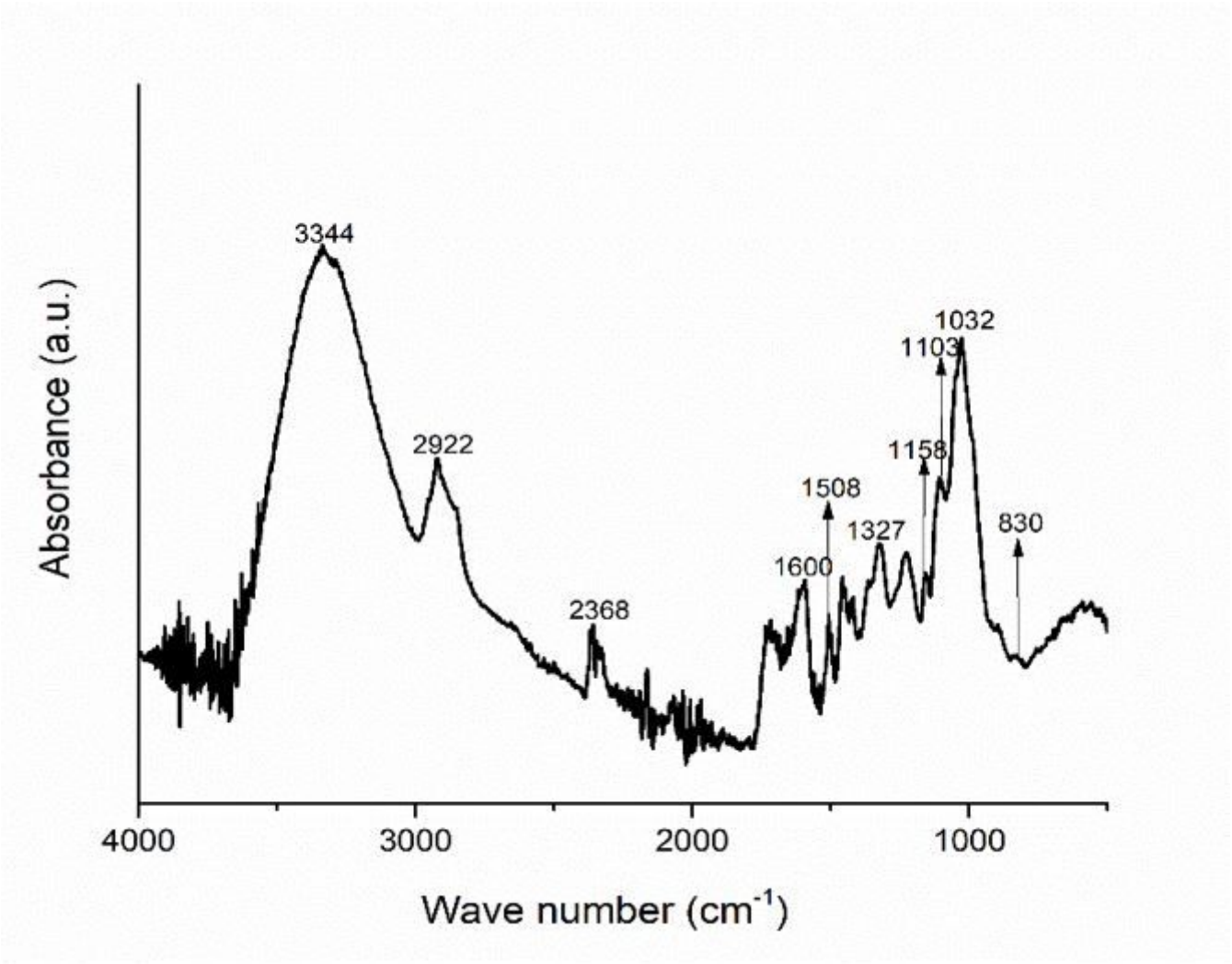

Figure 3

FTIR of pine sawdust waste.

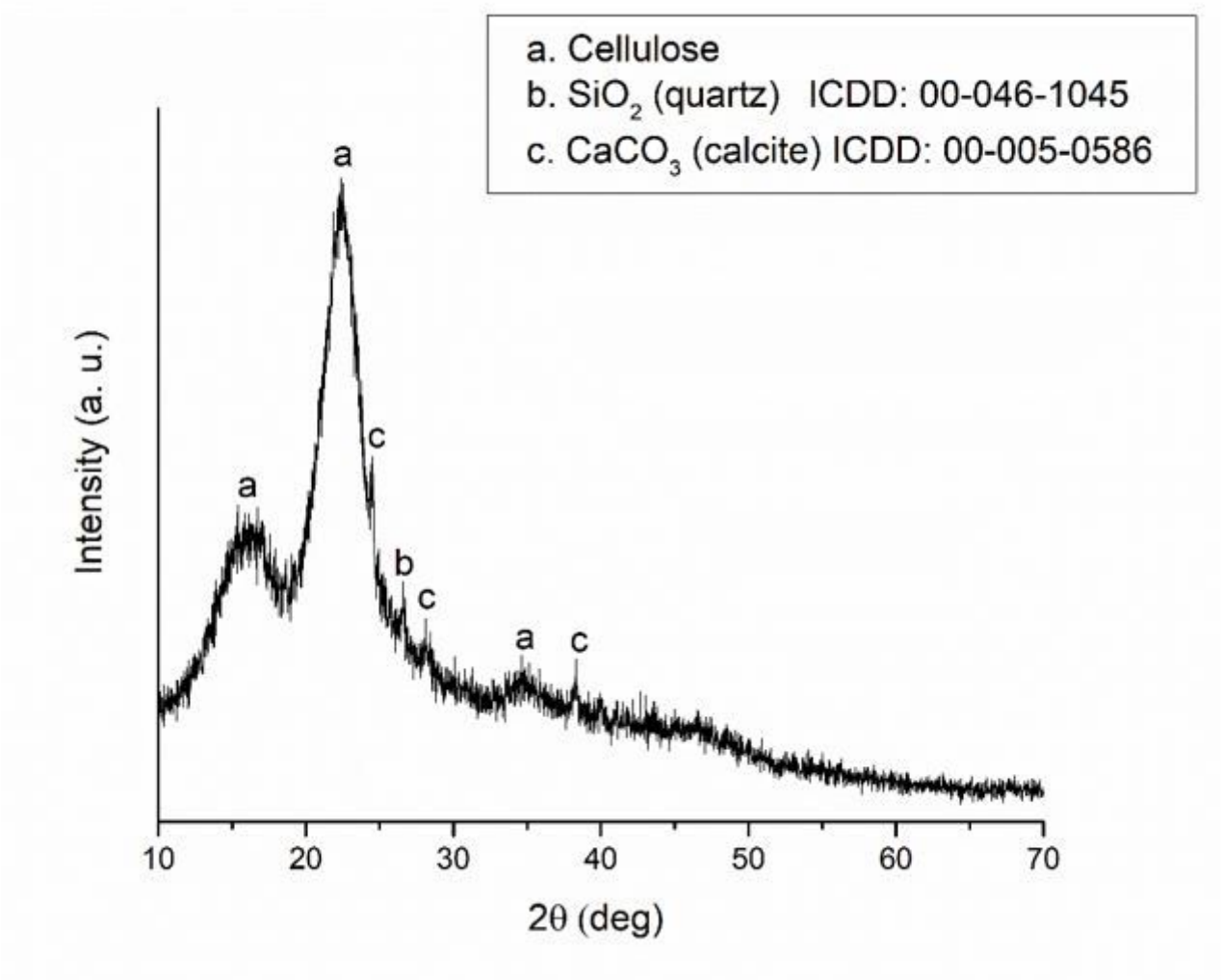

Figure 4

XRD diagram of the residual biomass of pine sawdust.

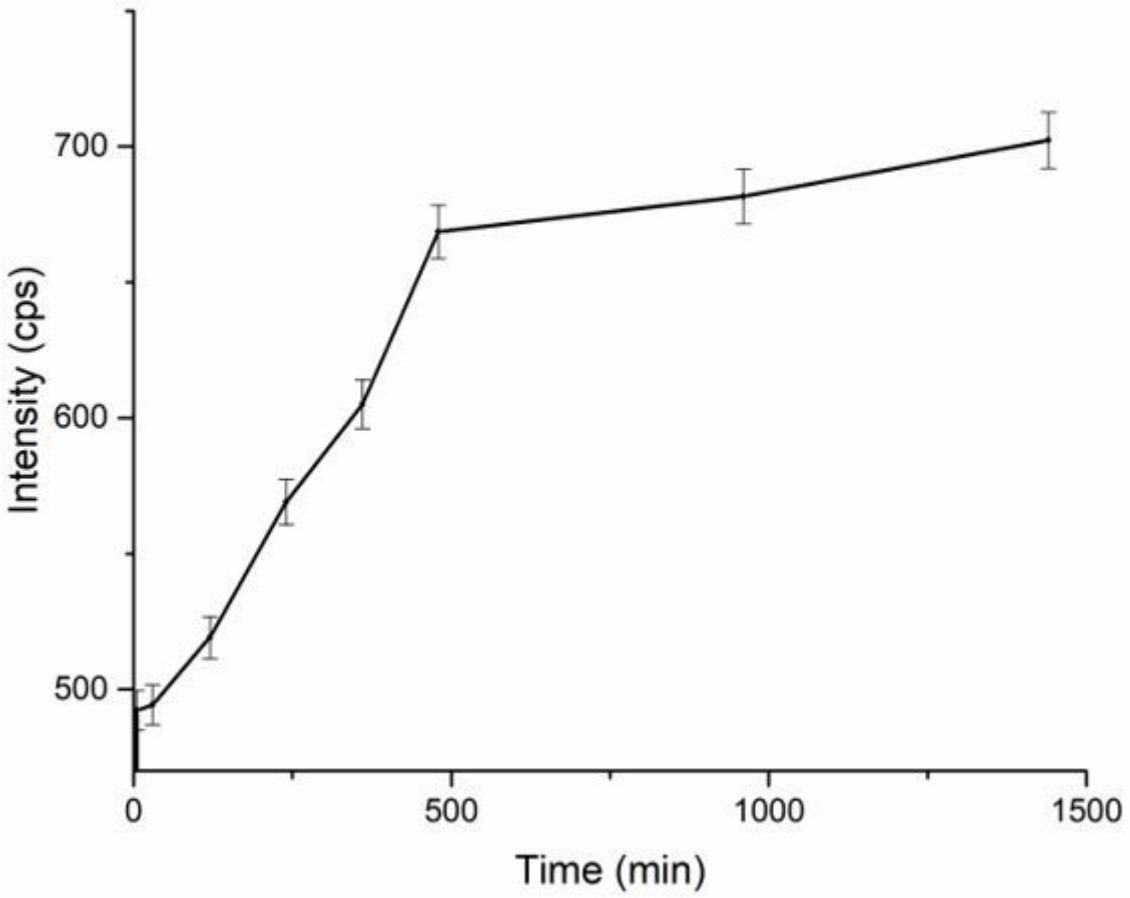

Figure 5

Study of Ni(II) adsorption as a function of time by XRF. 10 g L-1 of pine sawdust and initial NiCl2 concentration of 0.25 mg L-1.

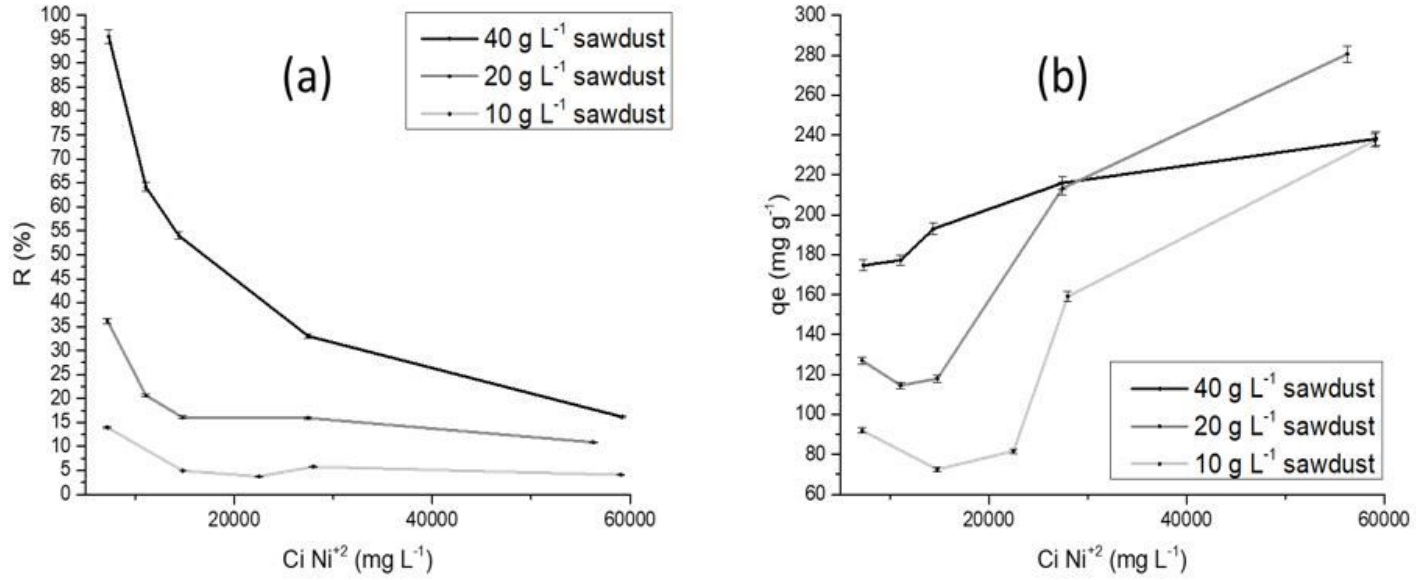

Figure 6

(a) R and (b) qe as a function of initial Ni(II) concentration for 10, 20 and 40 g L-1 of biomass

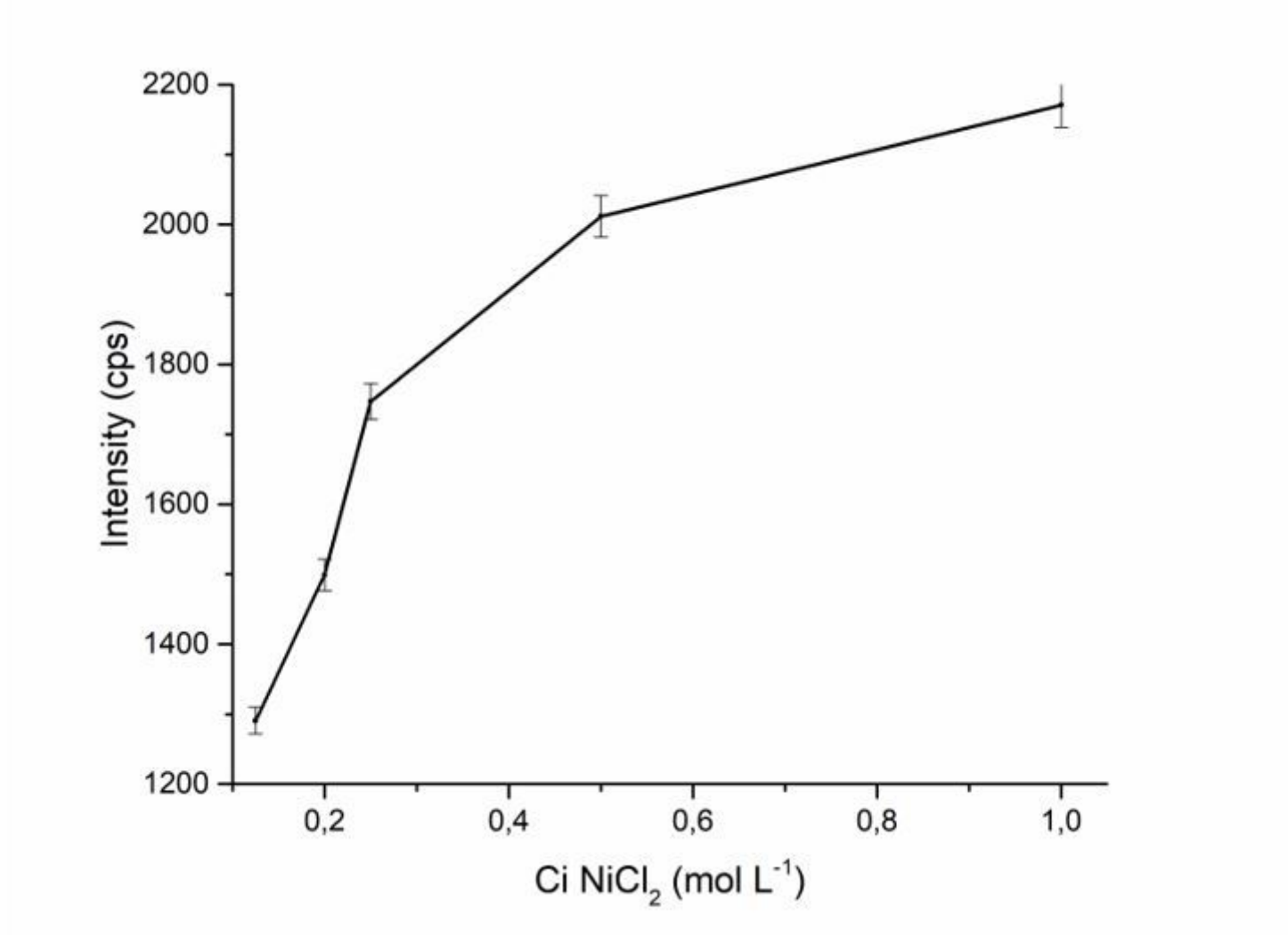

Figure 7

Intensity of Ni(II) adsorbed on 20 g L-1 of adsorbent measured by XRF and varying the initial concentration of NiCl2 solution.

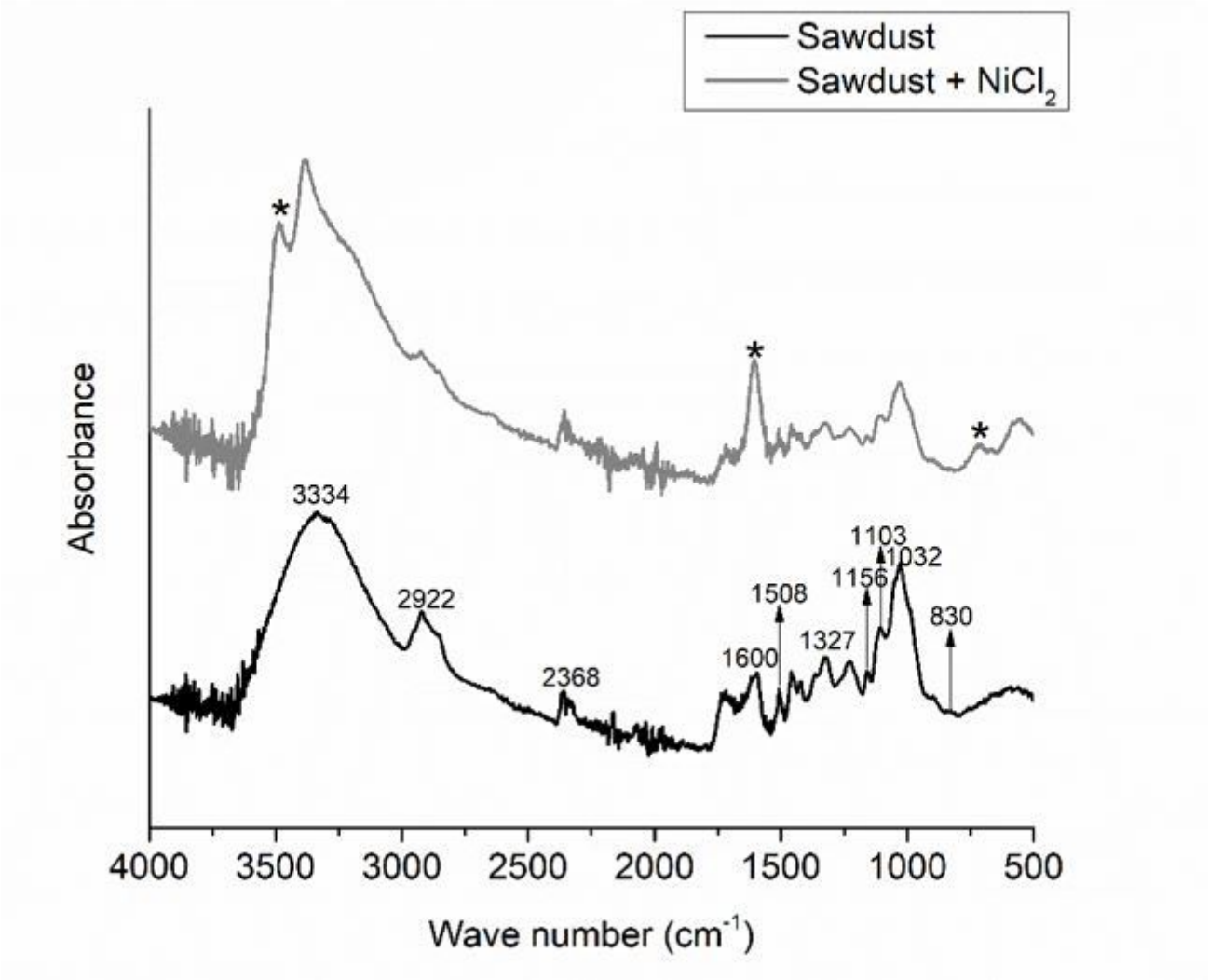

Figure 8

FTIR of native pine sawdust and residue treated with 1 mol L-1 NiCl2 solution.

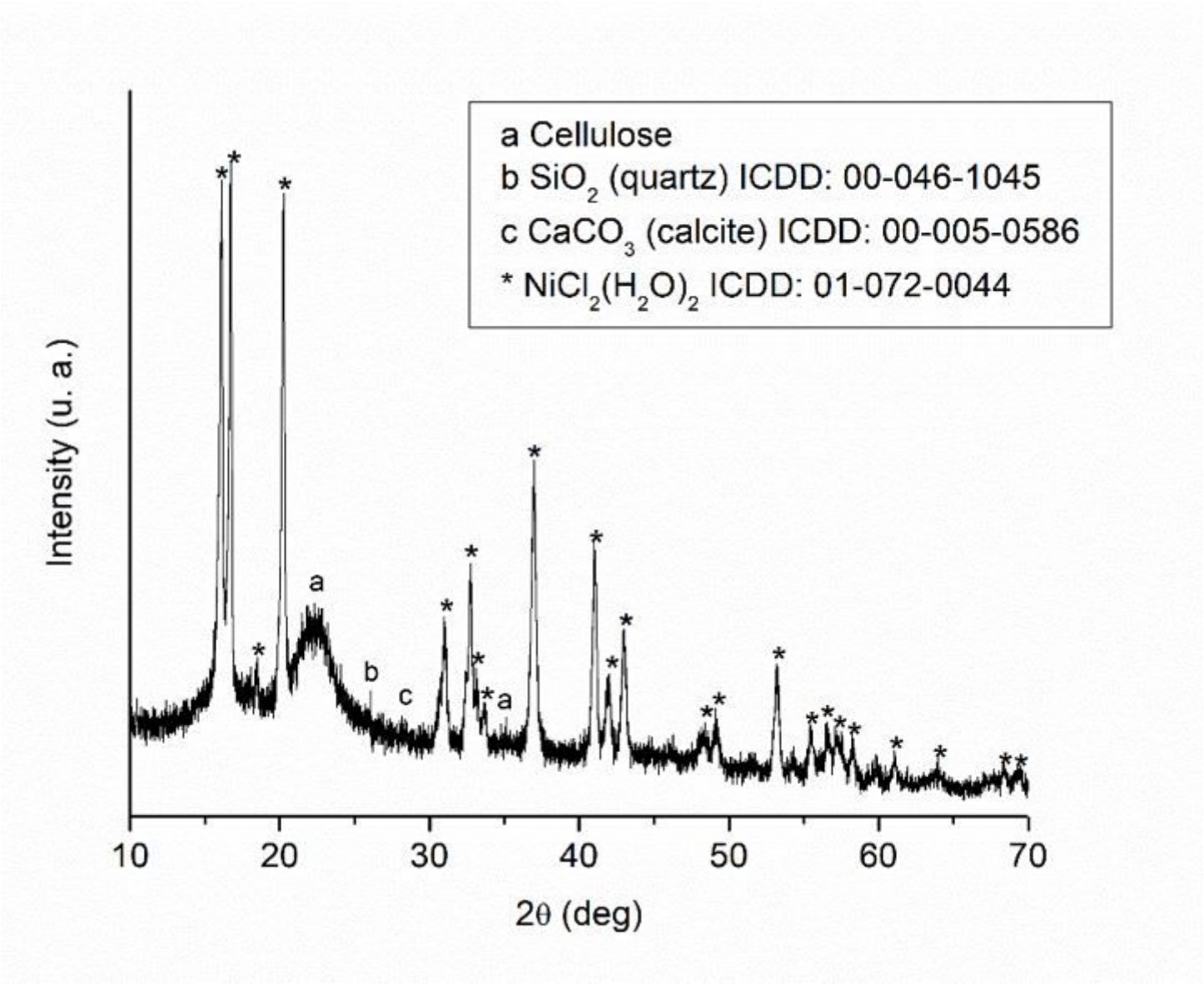

Figure 9

XRD of the pine sawdust after the adsorption treatment with a 1 mol L-1 NiCl2 solution.

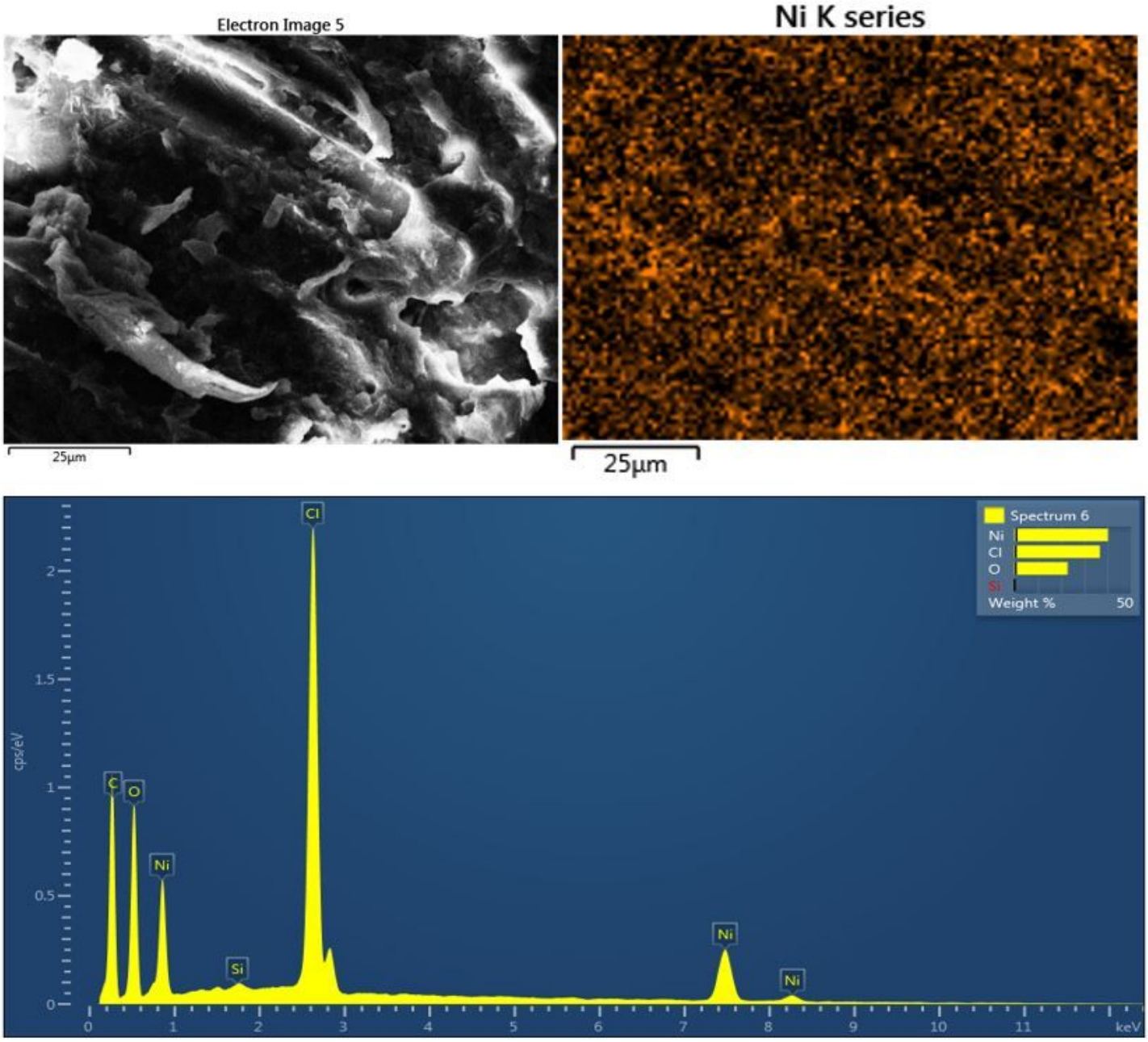

Figure 10

SEM-EDS of the pine sawdust after the adsorption treatment with a 1 mol L-1 NiCl2 solution.

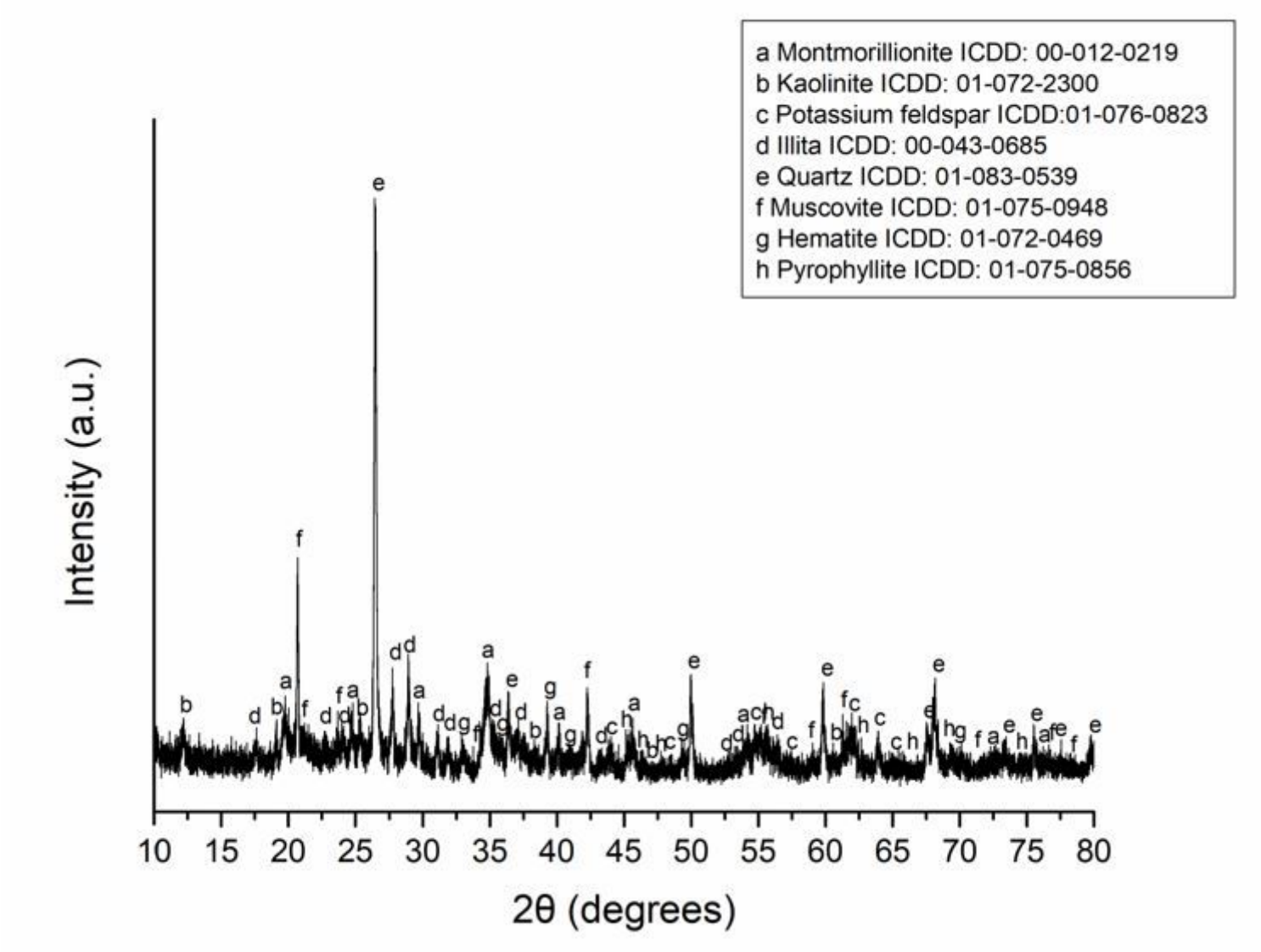

Figure 11

Composition of the clay by XRD.

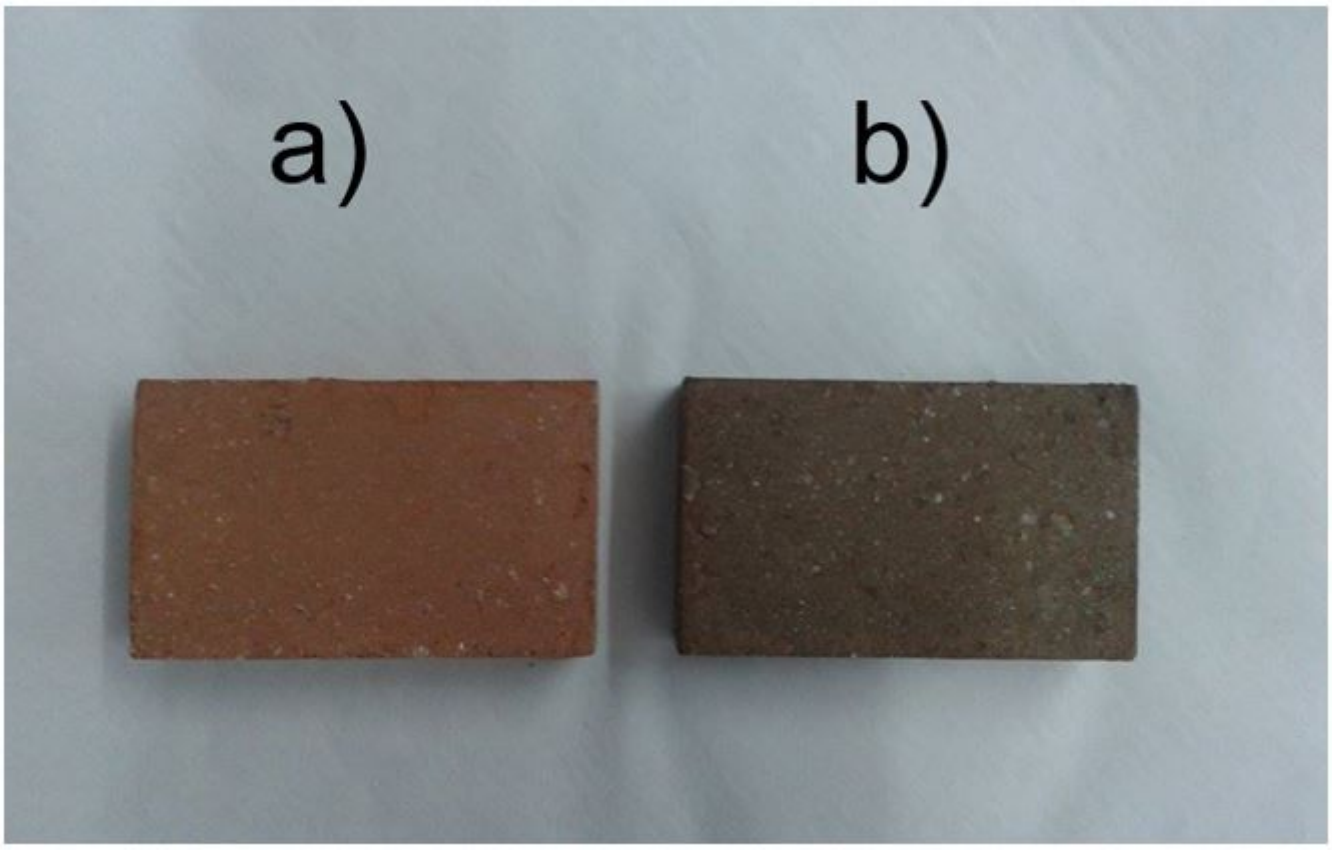

Figure 12

Macroscopic appearance (a) ARC y (b) AN20.

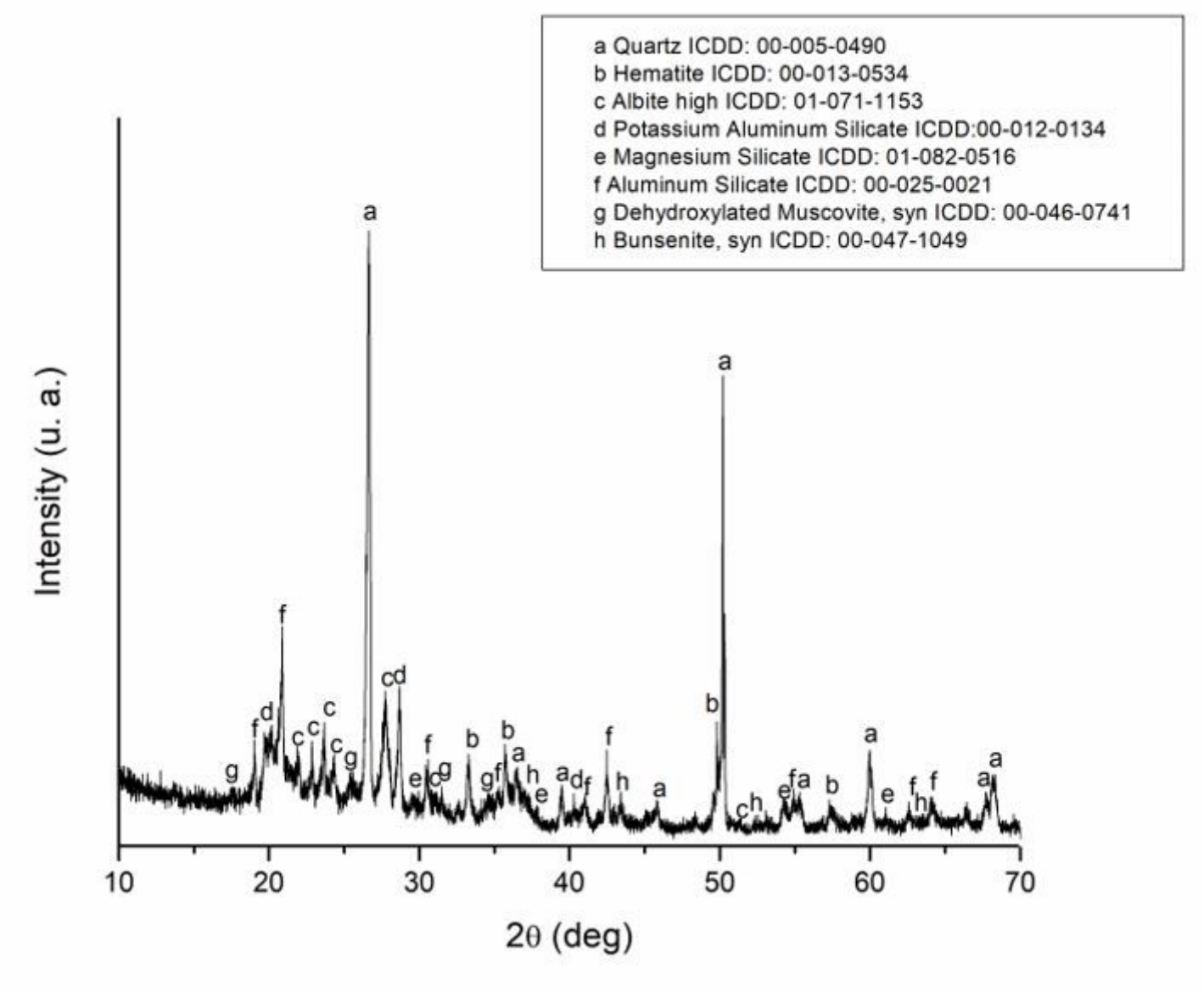

Figure 13

XRD of AN20 after calcination at 950 °C.

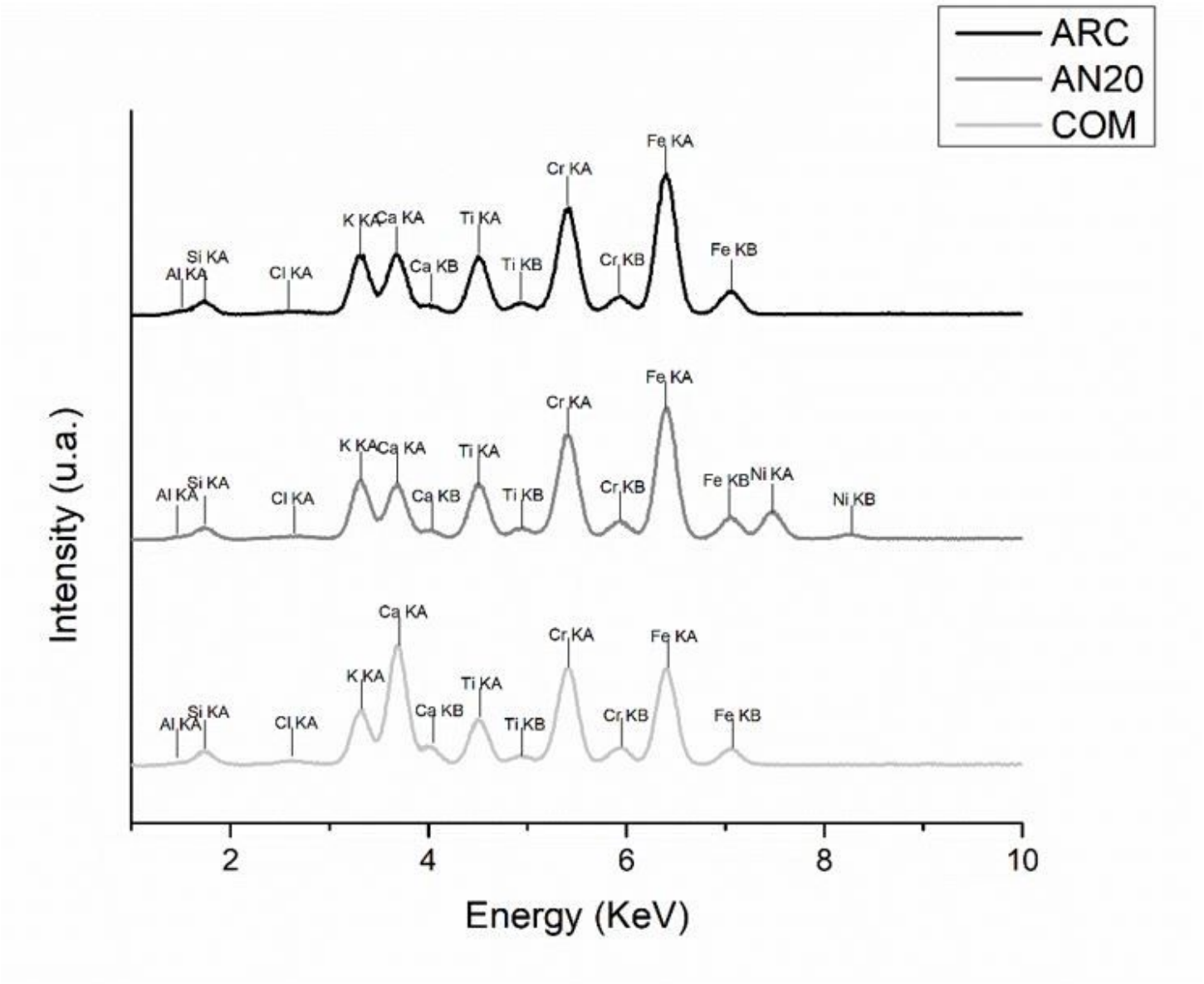

Figure 14

XRF of ARC, AN20 and COM after calcination at 950 °C.

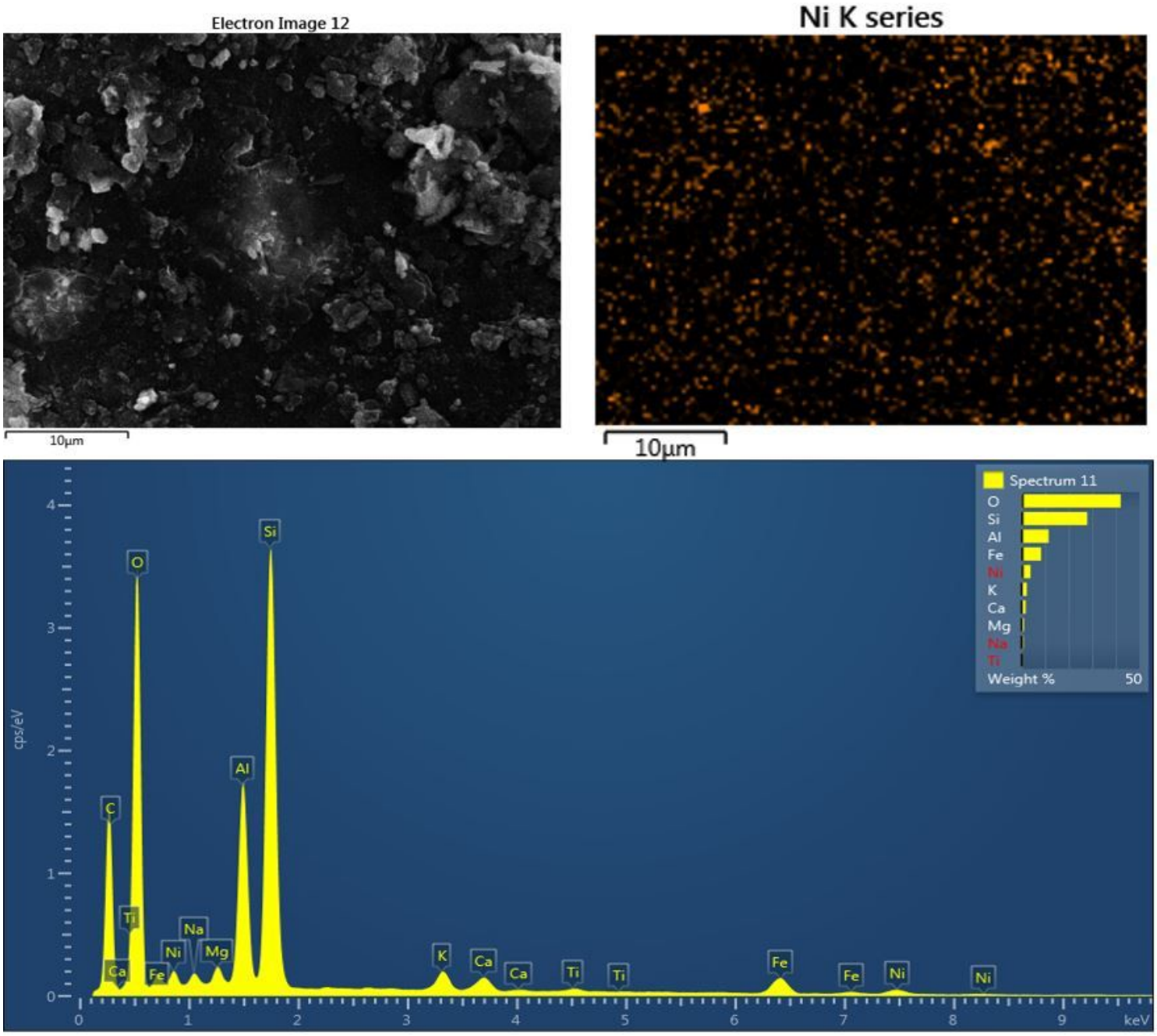

Figure 15

SEM-EDS of AN20 after calcination at 950 °C.

Supplementary Files

This is a list of supplementary files associated with this preprint. Click to download.

- formulas.docx